**FIG. 2.27. GRACE satellite observations of annual mean terrestrial water storage (the sum of groundwater, soil water, surface water, snow, and ice, as an equivalent height of water in cm) anomalies (2003–07 base period) by latitude.**

year. Other than continued replenishment of aquifers in the southeast, Australia reversed course from 2010, becoming wetter in the west and dryer in the northeast. Drought in equatorial Africa and recovery from drought in the Indochinese peninsula also stand out. Aquifers in central California (Famiglietti et al. 2011) and northern India (Rodell et al. 2009; Tiwari et al. 2009), which are stressed by groundwater pumping at
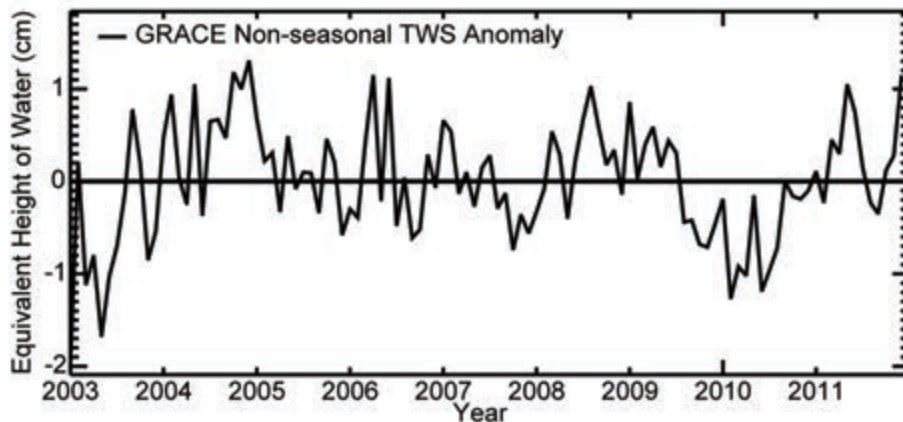
FIG. 2.28. As for Fig. 2.27 but for near-global average terrestrial water storage monthly mean anomalies (2003–07 base period) in cm equivalent height of water.

unsustainable rates, both raised their water levels in 2011. Significant reductions in TWS along the coast of Alaska, in the Patagonian Andes (also seen in Fig. 2.27), and in Greenland (see section 5f) and Antarctica (see section 6e) represent ongoing glacier and ice sheet ablation, not groundwater depletion.

Figures 2.27 and 2.28 show time series of zonal mean and global GRACE-derived non-seasonal, monthly mean TWS anomalies, excluding Greenland and Antarctica. Drying in the northern latitude band and wetting in the southern band in 2011 are clear

(Fig. 2.27). On average, Earth's land was relatively wet in 2011 (Fig. 2.28). From June 2010 to May 2011, global TWS increased by about 2.2 cm, which is equivalent to an 8 mm decline in mean sea level during that period (see Fig. 3.27), and TWS peaked again in December.

7) Soil moisture—R. A. M. De Jeu, W. A. Dorigo, R. M. Parinussa, W. W. Wagner, and D. Chung

Soil moisture retrievals from satellite observations are excellent indicators for climate variability because they integrate precipitation and evaporation. However, at large spatial scales the variation of soil moisture, in turn, affects evaporation and precipitation, via the water availability for evaporation and the subsequent partitioning of the Earth surface energy fluxes (Seneviratne et al. 2010).

Soil moisture has been globally observed from space since 1978 using microwave satellites (both passive and active), with a typical spatial resolution of about 0.25°. Satellite soil moisture represents the water content of the top few centimeters. Recently, a consistent multidecadal record of global soil moisture was developed by harmonizing and merging different satellite soil moisture datasets (Y. Y. Liu et al. 2012; see Sidebar 2.2). This homogenized dataset was used to calculate surface soil moisture anomalies for 2011 by subtracting the 1979–2010 climatology. Annual 2011 anomalies (Plate 2.1l) are predominantly positive in the Southern Hemisphere and negative in the Northern Hemisphere. Figure 2.29 reflects the major monthly hydroclimatic variations for 2011.

In early 2011, Australia suffered from several flooding events, especially in Queensland and Victoria, associated with La Niña conditions. From January to May the Okavango delta in southern Africa was completely flooded, resulting in a strong positive anomaly in the soil moisture data. This exceeded a
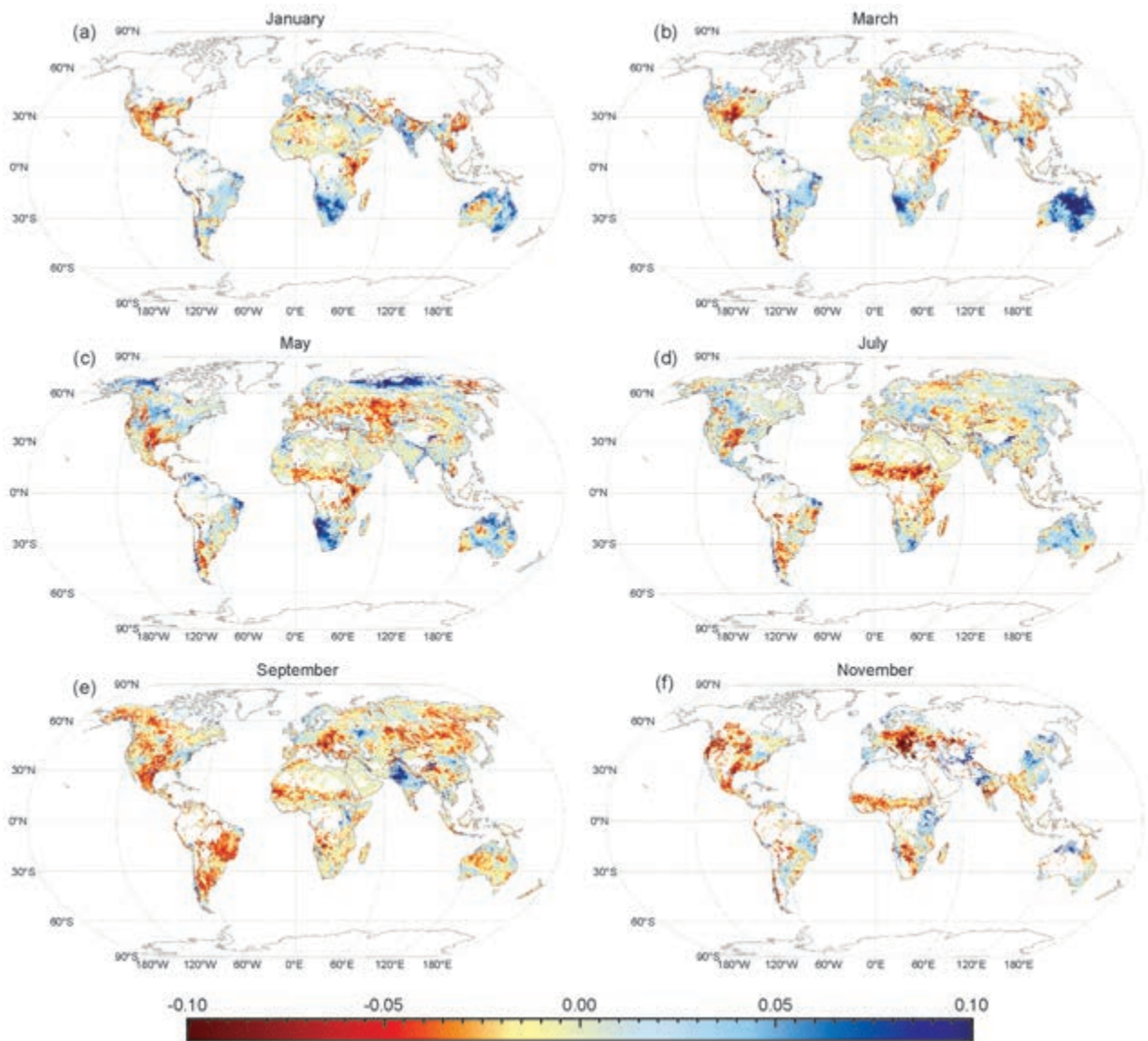
FIG. 2.29. Monthly soil moisture anomaly images for 2011 as derived from the multidecadal satellite soil moisture dataset. The anomalies are relative to a base period of 1979–2010. Note: The November anomaly image should carefully be interpreted; this image is solely based on ASCAT observations, because AMSR-E was switched off in October 2011.

similar flooding event in 2010 (De Jeu et al. 2011; Ives 2011). The delta is a large, flood-pulsed wetland and the flood was primarily caused by the seasonal flood wave of the Okavango River. Local rainfall variations played a smaller role. The flooding was asynchronous with the local rainy season and a result of interannual differences in local and upstream rainfall, as well as longer-term effects of surface-groundwater interactions within the delta (Wolski and Hudson 2008). The area of inundation displays a strong interannual variability, varying between 3500 km^2 and 14 000 km^2 (McCarthy et al. 2004; Gumbricht et al. 2004)

Following major flood events in 2010, Pakistan again experienced a series of flood events between July and September due to strong monsoonal rains. These are clearly visible in the September anomaly image of Fig. 2.29. However, the flood events of 2011 covered a smaller area than the events in 2010 (De Jeu et al. 2011).
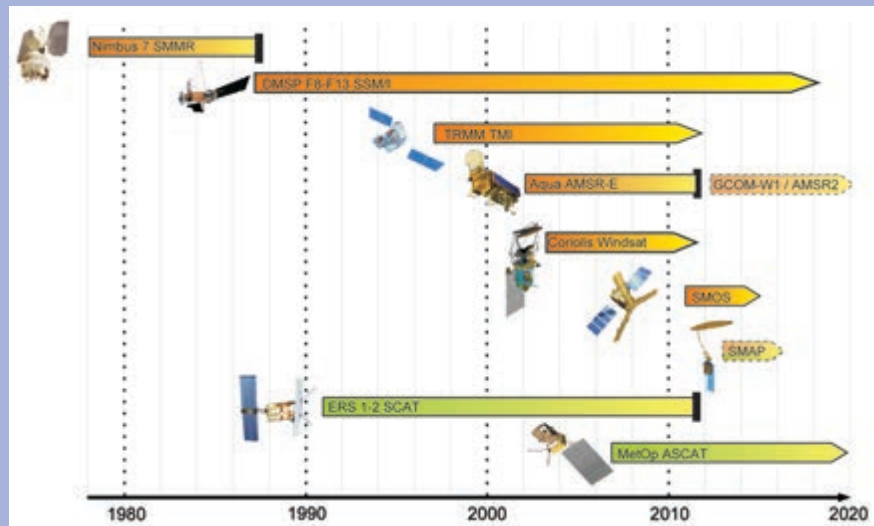
In 2011, three regions experienced severe droughts: the Horn of Africa, the southern US, and eastern Europe (see sections 7e, 7b, and 7f, respectively). The Horn of Africa drought became visible in soil moisture in March 2011 and persisted for the rest of the year. The southern US drought region showed a

Since the launch of the Nimbus-7 satellite in October 1978, there is a long legacy of satellite observations suitable for global soil moisture monitoring (Fig. SB2.4), but it took more than 20 years to develop the first satellite global soil moisture dataset. In 2002, a dataset was developed from scatterometer observations onboard the European Remote Sensing Satellites ERS-1 and ERS-2 (Wagner et al. 2003). Other research groups soon followed. De Jeu and Owe (2003) made a global soil moisture product from the historical Nimbus-7 SMMR data and Njoku et al. (2003) presented the first dataset based on AMSR-E observations.

Fɪɢ. SB2.4. Timeline of past, current, and future space-borne coarse resolution radiometers (orange) and scatterometers (green) suited for soil moisture retrieval on a global scale. (Source: updated version of Dorigo et al. 2010)

Today, numerous global soil moisture products from various satellites and research groups are freely available. These datasets vary in quality but all provide global soil moisture estimates of the top few centimeters at a rather coarse spatial resolution of 25 km–50 km (GCOS 2011). Global datasets are increasingly important in environmental research. For example, Liu et al. (2007) demonstrated the impact of El Niño on water resources in eastern Australia using TRMM soil moisture. Brocca et al. (2010) showed that runoff prediction for the Tiber River in Italy can be improved by incorporating ASCAT soil moisture, and Jung et al. (2010) used TRMM soil moisture to investigate a recent decline in global evaporation.

These different datasets are even more valuable if combined into one consistent multidecadal climate data record. This was addressed as part of the Water Cycle Multimission Observation Strategy (WACMOS) project from the Support To Science Element (STSE) program of the European Space Agency (ESA). Within this project, two extensively validated soil moisture products were selected to create a harmonized dataset; one from the Vienna University of Technology (TU Wien) based on active microwave observations (Wagner et al. 2003; Bartalis et al. 2007) and one from the VU University Amsterdam in collaboration with NASA, based on passive microwave observations (Owe et al. 2008). The harmonization of these datasets incorporates the strengths of both microwave techniques and spans continuously from 1978 onwards (Fig. SB2.4). However,
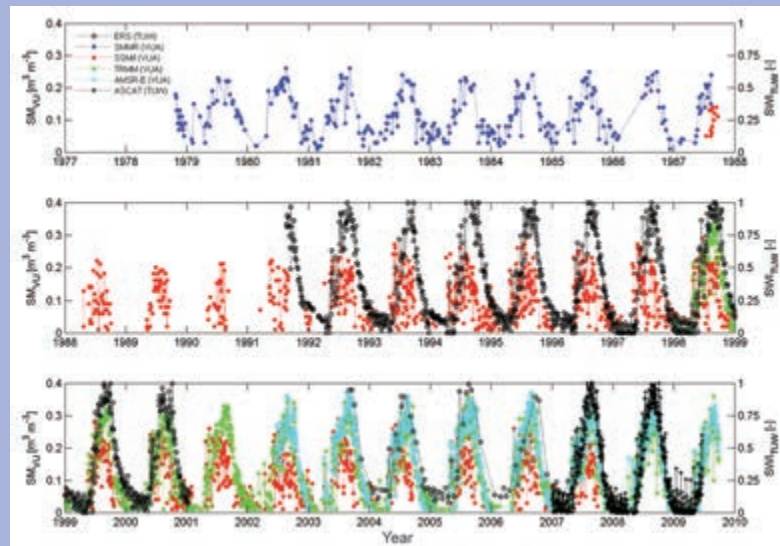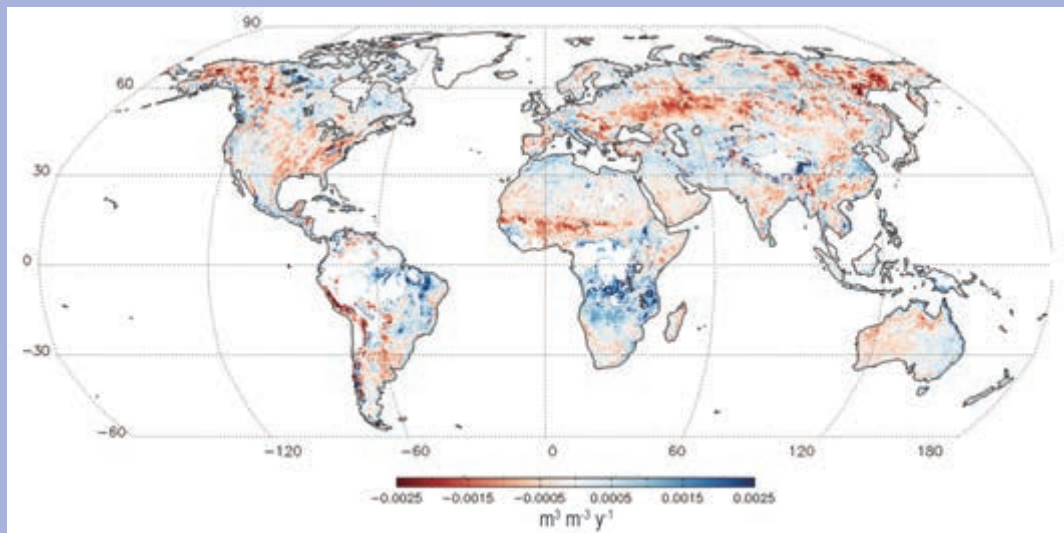
there were several challenges to developing such a dataset, e.g., differences in instrument specifications result in different absolute soil moisture values, the global passive and active microwave retrieval methods produce conceptually different quantities, and products vary in their relative performances depending on vegetation cover (Y. Y. Liu et al. 2012, manuscript submitted to *Remote Sens. Environ.*). This is clearly visible in Fig. SB2.5, where the original soil moisture retrievals from various satellites are plotted for a region in the Sahel. Here, both the active and passive soil moisture retrievals show similar seasonality but they have different magnitudes. TU Wien soil moisture retrievals are expressed as a degree of saturation (with a value between 0 and 1) while VUA retrievals are given in volumetric values ($m^3\ m^{-3}$). Besides this, the SSM/I-based estimates are less accurate than for the other sensors, owing to its limited soil moisture retrieval capabilities. It carries a Ku band (19 GHz) radiometer, which is less suitable for soil moisture retrieval than L (1.4 GHz), C (6.9 GHz), and X (10.7 GHz) band radiometers (Owe et al. 2008). A statistical methodology based on scaling, error characterization, ranking, and blending was developed to address these issues to create one consistent dataset (Liu et al. 2011, 2012). A third soil moisture dataset, provided by a land surface model (GLDAS-1-Noah), was used to scale the different satellite-based products to the same range. The blending of the active and passive datasets was based on their respective sensitivity to vegetation cover. While this approach imposes

the absolute values of the land surface model dataset to the final product, it preserves the relative dynamics (e.g., seasonality, interannual variations) and trends of the original satellite-derived retrievals (Y. Y. Liu et al. 2012). The ranking and blending strategy used does not increase the accuracy of the final product with respect to the merged ones, but allows a selective use of the most accurate measurements and increases the temporal density of the observations available. Finally, this method allows the long-term product to be extended with data from other current (e.g., SMOS) and future operational satellites and will be further improved as part of ESA Climate Change Initiative program (http://www.esa-cci.org/).

A simple trend analysis of this harmonized dataset is presented in Fig. SB2.6. Subtle soil moisture trends can be seen over the entire globe varying from -0.06 $m^3 m^{-3}$ to 0.06 $m^3 m^{-3}$ over the last 31 years. The strongest negative

FIG. SB2.5. Soil moisture over an area in the Sahel region (7°N, 12°E) according to different satellite observations. Note that soil moisture derivations from scatterometer sensors (indicated in black) are expressed as an index (right axis) and the VU soil moisture retrievals are expressed in $m^3 m^{-3}$ (left axis). (Source: De Jeu et al. 2009)

trends can be found in Russia, Kazakhstan, and the Sahel region. Strong positive trends are observed in northeastern Brazil and southern Africa. Most of these trends can directly be linked to the behavior of ocean oscillation systems. For example, the trends over Australia could be related to the polar movement of the Subtropical Ridge (STR), the Indian dipole, and the severe El Niño conditions within this period (Liu et al. 2007; Murphy and Timbal 2008; Y. Y. Liu et al. 2009).

FIG. SB2.6. Trends in annual average satellite soil moisture (in $m^3 m^{-3} yr^{-1}$), 1979–2010 base period. These values were derived from the harmonized soil moisture dataset, a 30+ year harmonized satellite soil moisture data record based on (historical) passive and active microwave observations.

negative anomaly throughout the year, and the Central and Eastern European drought was observable in the soil moisture data in November 2011.

8) Lake levels—C. Birkett and J.-F. Cretaux

Lake volumes are indirect indicators of climatic change because they respond to changes in precipitation integrated over their catchment basins. The response can be seen in open lakes and reservoirs but is particularly marked for closed lakes, i.e., those having no significant surface or subsurface outflow. Closed lakes can act as low-pass filters to variations in aridity, with a characteristic time constant of between 1 and 1000 years, depending largely on lake geomorphology. Deep lakes with steep shore topography are good proxies for high amplitude-low frequency changes, while shallow water basins are better indicators for rapid low-amplitude changes (Hostetler 1995). Lake variations can correlate with several modes of variability, e.g., ENSO, Indian Ocean, Pacific decadal, or North Atlantic Oscillations.

Research studies in 2011 continued to be regional or local in scope (Lee et al. 2011; Sarmiento and Palanisami 2011; Zhang et al. 2011), but global analyses require the systematic monitoring of all global lake volumes. Satellite imagery could provide changing lake surface area but currently no operational products exist. Satellite-based radar altimetry continues to provide surface water elevation products with datasets spanning 20 years (1992–2012). These lake level datasets can stand alone or be combined with ground-based measurements. They have varying temporal/spatial resolutions and varying accuracies, ranging from a few centimeters to tens of centimeters. Several web sites offer altimetric lake level products (e.g., NASA/USDA, ESA, LEGOS). The NASA/USDA website currently provides a first-order water-level status guide to drought or high water conditions in both lakes and reservoirs (Fig. 2.30). This is based on a mean nine-year lake level datum derived from a subset of the Topex/Poseidon dataset (1993–2002). Of the ~75 lakes, in February 2012, a third had below-average levels, another third above-average water levels. True climatic interpretation of the reservoir results are hampered by the magnitude of unknown anthropogenic effects. This status map at the NASA/USDA web site will be discontinued during 2012 as the operational program changes its policy to employ a datum based on a single date to enable an improvement in product accuracy. An ideal global lakes database would continue with such a level or volume
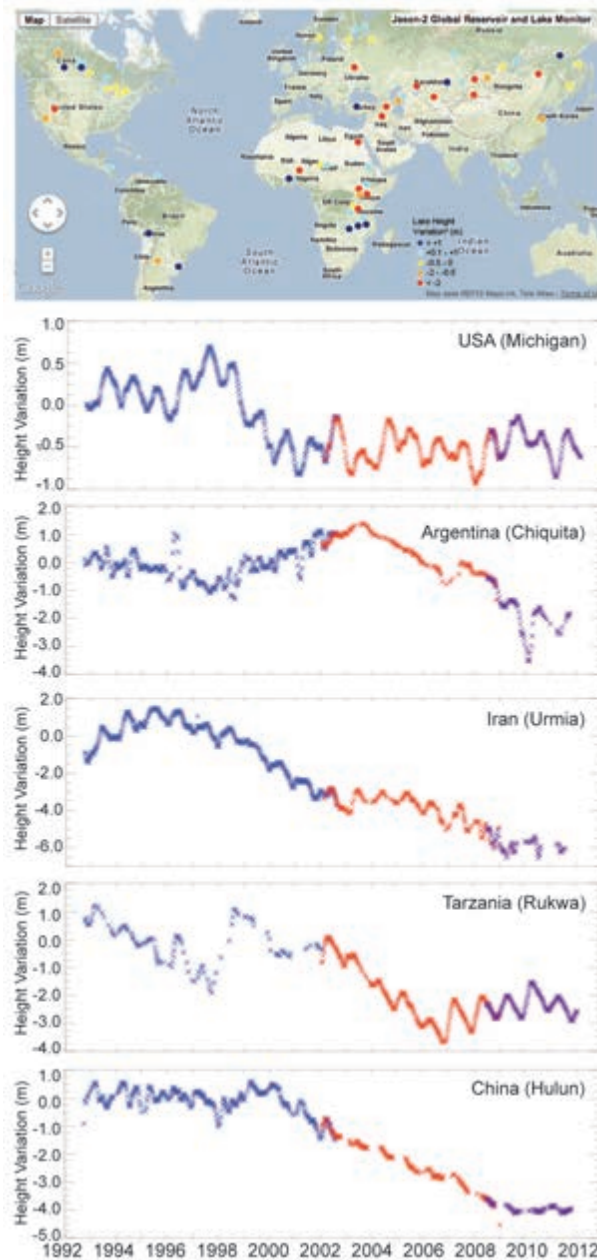
Fig. 2.30. (Top) Map showing the near-real-time (as of end of 2011) lake-level status of ~70 lakes with respect to a short-term mean (1993–2002). Red depicts low water drought and navy depicts high water. (Bottom) Examples of lake level time series (m) for five countries. (Source: USDA/FAS CropExplorer)

status indicator, as well as provide other parameters such as lake areal extent, surface water temperature and salinity, ice cover duration and thickness and basin-scale water storage anomalies. The type of lake included should also expand to include ephemeral lakes in both water-challenged and high latitude regions.